Improper origin of polar displacements at $CaTiO_3$ and $CaMnO_3$ twin walls

Paolo Barone,[1] Domenico Di Sante,[1,2] and Silvia Picozzi[1]
[1]*Consiglio Nazionale delle Ricerche, CNR-SPIN, I-67100 L'Aquila, Italy*
[2]*Department of Physical and Chemical Sciences, University of L'Aquila, Via Vetoio 10, I-67100 L'Aquila, Italy*
(Received 4 October 2013; revised manuscript received 26 February 2014; published 8 April 2014)

Recent interest in novel functionalities arising at domain walls of ferroic materials naturally calls for a microscopic understanding. To this end, first-principles calculations have been performed in order to provide solid evidence of polar distortions in the twin walls of nonpolar $CaTiO_3$ and magnetic $CaMnO_3$. We show that such polar displacements arise from rotation and/or tilting octahedral distortions—cooperatively acting at the twin wall in both considered systems—rather than from a proper secondary ferroelectric instability, as often believed. Our results are in excellent agreement with experimental observations of domain walls in $CaTiO_3$. In addition, we show that magnetic properties at the twin wall in $CaMnO_3$ are also modified, thus suggesting an unexplored route to achieve and detect multiferroic ordering in a single-phase material.

DOI: 10.1103/PhysRevB.89.144104 PACS number(s): 77.80.Dj, 71.15.Mb, 75.85.+t

I. INTRODUCTION

For a long time, domain boundaries in ferroelectric and ferroelastic materials have been looked at as mere juxtapositions of materials in the bulk state, lacking any interesting physical meaning on their own. In the last decade their role has been reconsidered, leading to the realization that domain walls (DWs) can display novel features which do not emerge in the bulk. As such, they can become active elements of potential new devices, leading to the "domain wall engineering" concept [1–4]. The emergence of new functionalities at domain walls can be loosely understood in the framework of the Landau theory of phase transitions. In fact, walls separate domains that are characterized by a primary order parameter (OP) pointing in two or more directions (polarities), implying that some component of the OP must monotonically decrease when approaching the domain boundary and eventually vanish at the wall. As a consequence, competing secondary order parameters, suppressed in the bulk, may in principle emerge in proximity of the boundaries [5–7].

A paradigmatic example of the competition between primary and secondary OPs has been put forward by the ferroelastic perovskite $CaTiO_3$ [8]. This material crystallizes at ambient conditions in a nonpolar *Pnma* structure (*Pbnm* setting adopted in the following) characterized by antiferrodistortive distortions (AFDs), which can be described as oxygen-octahedra tiltings and rotations, accompanied by a spontaneous ferroelastic strain. The parent cubic structure exhibits a secondary ferroelectric (FE) instability, namely a polar offcentering of Ti within the oxygen octahedral cages associated with the FE polarization [9]. Particularly interesting is the prediction of FE instabilities in magnetic $AMnO_3$ (A = Ca, Sr, Ba) [10–13] which questioned the usually invoked empirical "exclusion rule" for magnetic and FE perovskites [14], as experimentally confirmed in (Sr,Ba)MnO_3 [15] and strained $CaMnO_3$ thin films [16]. Therefore, the possibility of FE twin walls in this class of magnetic compounds may represent a new and unexplored route to achieve nanoscale multiferroic features in single-phase materials. Furthermore, a significant magnetoelectric coupling may be expected, since both magnetism and FE features would originate from the very same B-site ions.

In principle, the presence of twin ferroelastic domains in $CaTiO_3$ could imply a suppression of the primary AFD OP at the domain wall and a consequent activation of the secondary FE instability. This motivated recent numerical calculations based on an atomic-scale, though empirical, description of the wall, predicting ferrielectricity at $CaTiO_3$ twin boundaries, with maximum dipole moments appearing at the wall [8]. Very recently, a direct observation of such ferrielectric domain boundaries in $CaTiO_3$ was achieved by transmission electron microscopy [17], reporting, however, offcentric displacements one order of magnitude larger than those theoretically predicted. More importantly, the simple interpretation based on the coexistence or competition of primary and secondary OPs may not really apply to $CaTiO_3$, since the AFD distortions never fully disappear in the experimentally observed twin walls, while the polar offcenterings have been found to be strongly locked to the twin angle and local pattern of AFD distortions. These observations apparently suggest an improper origin for the emerging DW ferroelectricity, hindering the possibility of switching its polarization via an applied electric field. On the other hand, a sizable DW electric polarization could serve in principle as an additional handle for, e.g., controlling twin-wall dynamics.

Motivated by these premises, we performed an accurate analysis of DWs in both $CaTiO_3$ (CTO) and $CaMnO_3$ (CMO) in the framework of first-principles density-functional-theory (DFT) calculations. We find that polar offcenterings are caused by the peculiar interplay of cooperative AFD rotations at the wall, rather than by the activation of a secondary FE instability. Microscopically, the mechanism can be viewed as a local realization of the recently proposed hybrid improper ferroelectricity [18–20]. In this framework, the AFD pattern of tilting and/or rotations of BO_6 octahedra is expected to cause antipolar offcenterings of A-site cations [19,20]; as a consequence, twin boundaries in perovskite oxides could play the role of walls between domains with different antipolar distortions, implying in principle a non-negligible contribution of A-site cations to the wall polarization. On the other hand, a significant contribution to polarization is predicted to originate as well from B-site ions that offcenter significantly even in the presence of a magnetic ordering (an unexpected effect for

CMO at ambient conditions) in response to the local pattern of AFD distortions at the DW.

II. METHODS AND COMPUTATIONAL DETAILS

We adopted the PBEsol generalized-gradient approximation for the exchange-correlation functional revised for solids [21] as implemented in the VASP code [22], using a 500 eV plane-wave cutoff and a 1×4×4 Monkhorst-Pack mesh. Cell and ionic relaxations have been performed until forces acting on ions were smaller than 0.01 eV/Å. Furthermore, as CMO is a G-type antiferromagnetic (AFM-G) insulator in its orthorhombic ground state [23], we impose the AFM-G spin-ordering away from the wall, while allowing for different types of parallel- and antiparallel-spin bonds at the interface. Since two DWs are needed to implement periodic boundary conditions, large supercells have been built comprising 16 pseudocubic ABO_3 unit cells along a direction X perpendicular to the wall and 2 unit cells along directions Y and Z parallel to the wall, for a total of 320 atoms. Different domains may be identified by defining the primary rotational order parameter as an axial vector Φ from the static rotational momenta $\boldsymbol{\phi}(\boldsymbol{R}) \propto \sum_{l=1,6} \hat{\boldsymbol{r}}_l \times \hat{\boldsymbol{r}}_l'$ [24]. Here, $\boldsymbol{R} = i\boldsymbol{a}_X + j\boldsymbol{a}_Y + k\boldsymbol{a}_Z$ is the B-site supercell lattice vector, while $\hat{\boldsymbol{r}}_l$ ($\hat{\boldsymbol{r}}_l'$) represents oxygen positions within each BO_6 octahedron before (after) the static rotation about an axis passing through the BO_6 center of mass. The cCartesian components x,y,z of the axial vector $\boldsymbol{\phi}(\boldsymbol{R})$ correspond to rotations about corresponding axes X,Y,Z. The order parameter for each layer parallel to the DW is then defined by including appropriate phase factors as

$$\Phi_{x,y}(X) = (-1)^i \frac{1}{4} \sum_{j,k} (-1)^{j+k} \phi_{x,y}(\boldsymbol{R}), \tag{1}$$

$$\Phi_{z}(X) = (-1)^i \frac{1}{4} \sum_{j,k} (-1)^{j} \phi_{z}(\boldsymbol{R}), \tag{2}$$

corresponding to the general $a^-b^-c^+$ rotational pattern in Glazer's notation [25].

III. RESULTS

A. Domain wall structure and polarization profile

After ionic relaxations, the energetically more favorable DW is a ferroelastic wall obtained through a mirror twin law about the $(1\bar{1}0)$ plane of the $Pbnm$ structure, in agreement with the experimental observations [17], with an estimated DW energy $E_{DW} = 16$ (41) mJ/m^2 for CTO (AFM-G CMO) [26]. The twin wall is characterized by a switching of the out-of-phase BO_6 rotations around the supercell X axis at the wall [27] as described by $\Phi_x(X) \propto \tanh(\frac{X}{\xi})$ (see Fig. 1). After cell relaxation, a twin angle of 181.2° is found for CTO, in excellent agreement with experimental findings [17]. In Figs. 1(c) and 1(d) we show the layer-averaged offcentering $\boldsymbol{D}^{\mathrm{Ti(Mn)}} = \frac{1}{4} \sum_{j,k} \boldsymbol{d}^{\mathrm{Ti(Mn)}}(\boldsymbol{R})$ of Ti (Mn), where $\boldsymbol{d}^{\mathrm{B}}(\boldsymbol{R}) = \frac{1}{6} \sum_{l=1,6} (\boldsymbol{r}^B - \boldsymbol{r}_l^O)$ describes the local displacement of B-site ions with respect to the center of mass of each BO_6 octahedron. Two ion offcenterings clearly appear at the wall: a polar distortion along DW direction Y as large as 6.5 pm (0.7 pm) for CTO (AFM-G CMO), and an antiphase

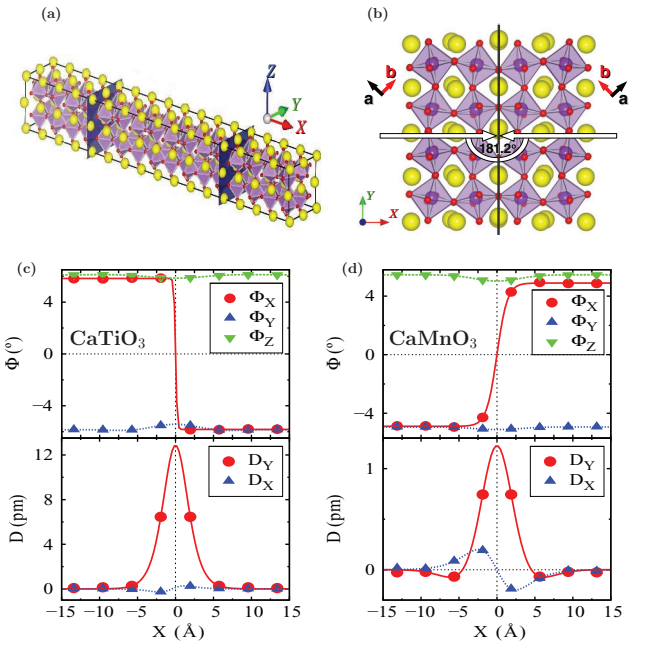

FIG. 1. (Color online) (a) Ball-and-stick model of a CaTi(Mn)O_3 supercell. (b) Top view highlighting the ferroelastic domains, with orthorhombic cells mirrored with respect to the $[1\bar{1}0]$ plane, and the twin angle of $CaTiO_3$. Yellow and red balls refer to Ca and O atoms, respectively, while Ti (Mn) ions are inside purple octahedra. (c),(d) Layer-averaged rotational order parameters as a function of the distance from the twin wall and associated offcentering of B-site ions estimated from the center-of-mass of oxygen octahedra for (c) CTO and (d) CMO. The DW profile of the polar offcenterings was fitted via a function $D_y(X) = D_0\,\mathrm{sech}^2\left(\frac{X}{\xi_D}\right)$ [7].

(odd) polarization developing perpendicularly to the wall. Interestingly, if we define the Ti (Mn) offcenterings with respect to Ca sites (as done in Ref. [17]), the sign of the Ti (Mn) displacement along Y is reversed, amounting to $\simeq -6.2$ pm (-3.1 pm). If on one side the magnitude of the effect is again in excellent agreement with the experimental value 6.1 pm, the change of sign suggests that actually also Ca ions are displaced with respect to oxygens. Indeed, one can also define the Ca offcentering from the center of mass of a dodecahedral cage AO_{12} as $\boldsymbol{d}^{\mathrm{Ca}}(\boldsymbol{R}) = \frac{1}{12} \sum_{l=1,12} (\boldsymbol{r}^{\mathrm{Ca}} - \boldsymbol{r}_l^{\mathrm{O}})$, finding a layer-averaged offcentering of Ca with respect to the Os as large as 21.7 pm (6.8 pm) along the Y direction at the CTO (AFM-G CMO) DW.

In order to get a deeper insight on the distortions close to the twin boundary, we evaluated the polarization profile from the unit-cell polarization

$$\boldsymbol{P}^{(i)} = \frac{e}{\Omega_c} \sum_{\alpha} w_a \boldsymbol{Z}_{\alpha}^* \cdot \boldsymbol{u}_{\alpha}^{(i)}. \tag{3}$$

Here e is the electron charge, Ω_c is the volume of a five-atom (bulk) unit cell, $\boldsymbol{Z}_{\alpha}^*$ are the Born effective charge tensors, and $\boldsymbol{u}_{\alpha}^{(i)}$ describes the ionic displacement of ion α from its bulk position in unit cell i. [28] The coefficients w_α account for the possible overcounting of ionic contributions, since some of the ions in the five-atom unit cell are shared by neighboring cells, and depend on the choice of the unit cell. We adopted

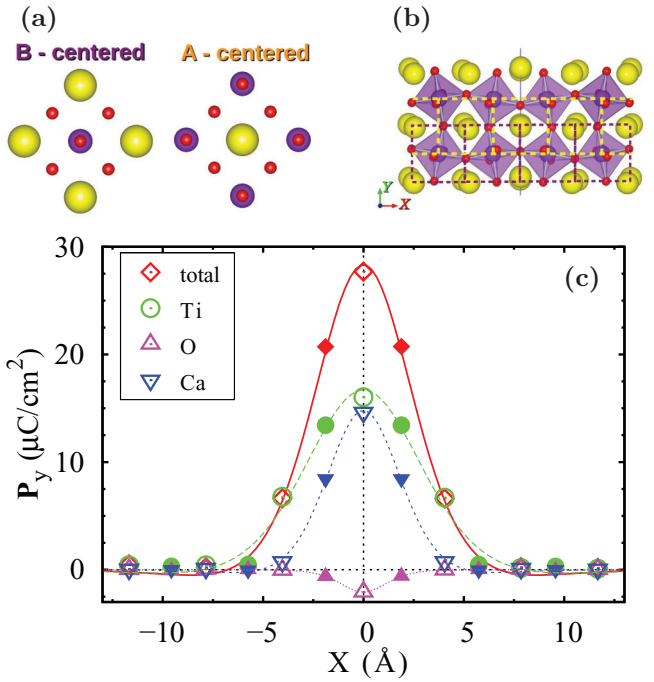

FIG. 2. (Color online) (a) Sketch of the two different choices of unit cells used for the calculation of polarization via Born effective charges. The polarization profile in the supercell is then evaluated as sketched in (b). (c) Total polarization profile at the CTO twin wall and contributions assigned to different ions; empty and solid symbols refer to different choices of the unit cell, referring respectively to A-site and B-site centered cells.

two choices [shown in Fig. 2(a)], namely a B-site centered, with a Ti (Mn) ion sitting in the center of the unit cell, and an A-site centered cell, where a Ca ion is located at the center of the cell. In the first case, each of the six neighboring oxygens is shared by two unit cells, whereas each Ca ion is shared by eight unit cells, implying $w_O = 1/2$ and $w_{Ca} = 1/8$ (weight factors for A-centered cells are analogously chosen as $w_O = 1/4$ and $w_B = 1/8$). Within this formulation, the origin of the reference frame can be arbitrarily chosen, since only relative displacements are taken into account; furthermore, the contribution to total $\boldsymbol{P}$ due to each individual ion can be unambigously identified, corresponding to Eq. (3) where only terms relative to the chosen ion are included. In Fig. 2(a) we show the layer-averaged polarization profile for a CTO DW, where both Ca and Ti ions are shown to contribute significantly to the total $\boldsymbol{P}$, resulting in a DW polarization as large as 27.7 μC/cm^2.

B. Improper origin of domain wall polarization

The Ca contribution to $\boldsymbol{P}$ can be understood in terms of coupled AFD rotational modes. By taking into account symmetry-allowed trilinear couplings with general expression $\Phi_\alpha \Phi_\beta D_\gamma$, in fact, it has been shown that the $a^-a^-c^+$ pattern adopts two kinds of antipolar displacements of A-site ions [20] as shown in Figs. 3(a) and 3(b). The first type, $\boldsymbol{A}^{001}$, involves A-ion displacements along $[110]_{pc}$ directions of the pseudocubic cell, modulated in antiphase when going from a (001) CaO plane to an adjacent one; in terms of $\boldsymbol{d}^{\mathrm{Ca}}(\boldsymbol{R})$ it can

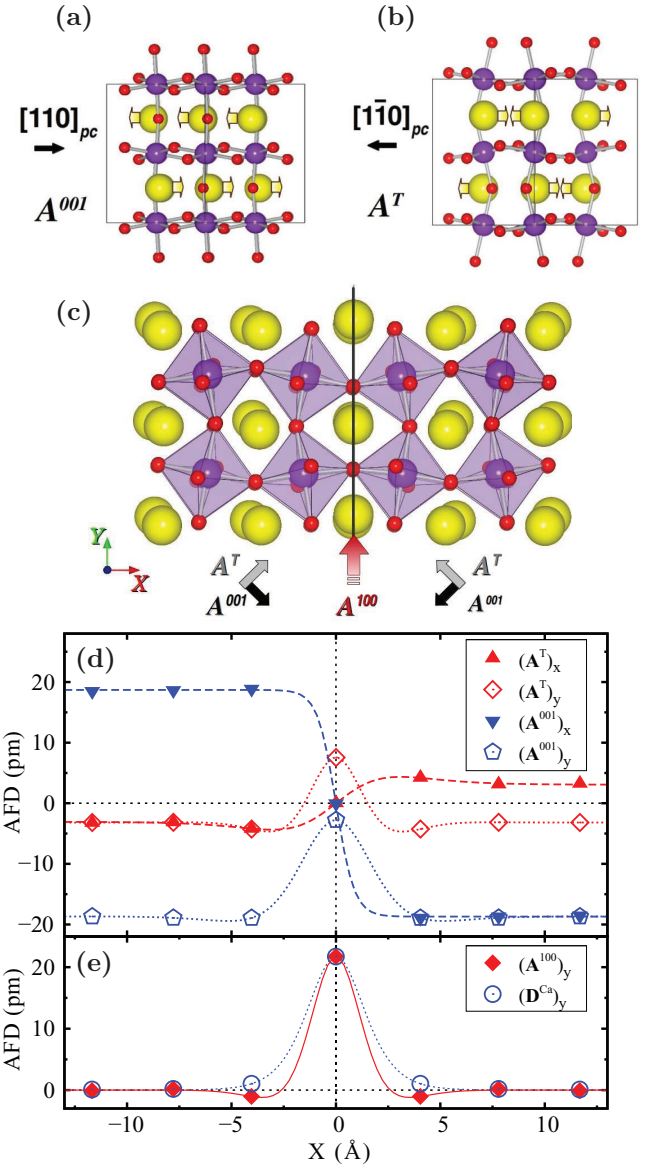

FIG. 3. (Color online) Antipolar displacements of Ca ions in the bulk $Pbnm$ structure of $CaBO_3$, showing the two kinds of modulated collective antiferrodistortive distorsions (a) $\boldsymbol{A}^{001}$ and (b) $\boldsymbol{A}^T(X)$. (c) Antipolar displacements at the considered twin wall, separating two twin domains characterized by different AFD polarizations; the emergence of the third local displacement induced by the local rotational pattern is also highlighted. (d) DW profile of bulk antipolar order parameters in CTO, describing antipolar displacements of Ca ions evaluated in the local center of mass of each CaO_{12} dodecahedron. (e) Layered-averaged polar offcentering $\boldsymbol{D}^{\mathrm{Ca}}$ of Ca ions, compared with the DW profile of the antipolar OP $\boldsymbol{A}^{100}$ that is expected to develop only at the wall.

be expressed as

$$\boldsymbol{A}^{001}(X) = \frac{1}{4}\sum_{j,k}(-1)^k\, \boldsymbol{d}^{\mathrm{Ca}}(\boldsymbol{R}). \tag{4}$$

The second type, $\boldsymbol{A}^T(X)$, occurs along the $[1\bar{1}0]_{pc}$ direction and has an antiphase modulation along the three pseudocubic

directions, reading

$$A^T(X) = (-1)^i \frac{1}{4} \sum_{j,k} (-1)^{j+k} d^{\mathrm{Ca}}(\boldsymbol{R}). \quad (5)$$

Their profile across the DW is shown in Fig. 3(d), suggesting that the twin boundary represents in fact a wall between domains with different antipolar polarities; specifically, the X component of both the antipolar OPs vanishes at the boundary and is opposite in different ferroelastic domains as shown in Fig. 3(c). A third antipolar distortion $A^{100} = (-1)^i \frac{1}{4} \sum_{j,k} d^{\mathrm{Ca}}(\boldsymbol{R})$ is also predicted to be induced by the local AFD distortions at the DW [27], involving displacements along the $[010]_{pc}$ direction which are modulated in antiphase as one moves from a (100) CaO plane to the next one. As shown in Fig. 3(e), the major contribution to the Ca displacements comes in fact from this mode. On the other hand, once the inversion symmetry is locally broken by the AFD DW, the FE instability of B-site ions is easily activated, *but only along the directions dictated by the primary non-polar distortions (rotations)* causing the symmetry breaking [29]. Thus, a significant displacement of B-site ions occur parallel to the Y axis, while the switching of the X component of the Ca motions across the wall causes the antiphase (odd) modulation of $D_x^B(X)$. Such offcentering distortions are typically smaller than those of Ca ions; it is worth noting, however, that both Ti and Mn show anomalous Born effective charges ($Z^*_{\mathrm{Ti},yy} = +7e$ and $Z^*_{\mathrm{Mn},yy} = +6.8e$), thus contributing significantly to the DW electric polarization. Eventually, the devised improper origin of DW polarization easily explains the observed locking of the ionic offcentering to the twin angle and local AFD rotational pattern. Following Ref. [20], the most relevant coupling between distortional modes at the wall is found to occur trilinearly between d_y^{Ca},ϕ_x, and ϕ_y. In principle, the polar distortion could be reversed by reversing one of these two rotational momenta, a possibility hardly attained in a realistic case due to the cooperative character of rotational distortions that would require a reversal of the rotational pattern in the whole domain. Nonetheless, this situation is realized in our supercell where the two symmetric DWs are characterized by exactly the same ϕ_y (and ϕ_z) but opposite ϕ_x, and where the polarization profile is indeed found to be reversed.

C. Magnetic exchange at the domain wall

As for CMO, an interesting additional degree of freedom is brought about by the localized magnetic moments on Mn ions. If, on one hand, all previous considerations perfectly apply to the case of a single magnetic domain (with ground-state AFM-G configuration), on the other hand significant spin-phonon coupling effects may be expected at CMO DWs. [30] We considered then a selection of possible interface spin configurations, with parallel-spin bonds along the X, Y, or Z direction. As expected, all these spin configurations resulted in higher energies as compared to the AFM-G single domain after ionic relaxation; the FM_X configuration shown in Fig. 4(a), that corresponds to a truly magnetic domain wall (MW) between two AFM-G domains with opposite polarities, results in the second lowest DW energy, namely $E_{DW+MW} = 46\ \mathrm{mJ/m^2}$, with an energy increase of $\sim 5\ \mathrm{mJ/m^2}$ with respect to the AFM-G DW. The structural-induced modifications of

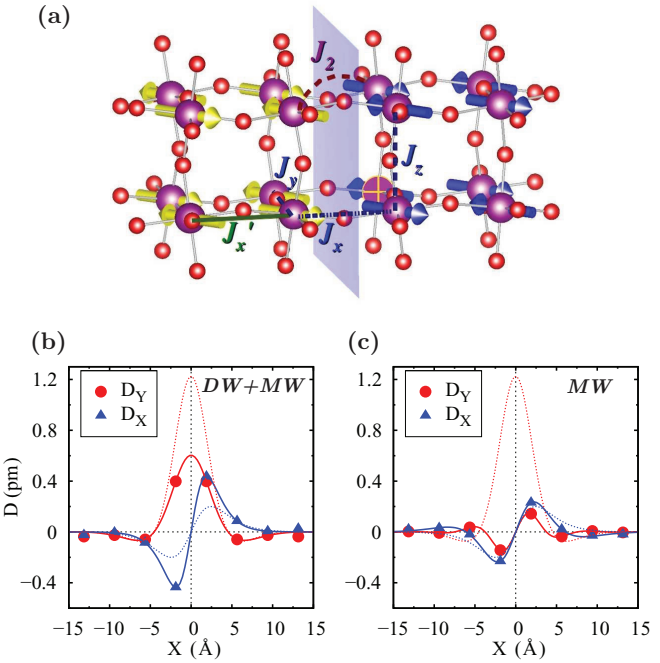

FIG. 4. (Color online) (a) Sketch of the evaluated DW exchange couplings at the interface; the domain wall between two AFM-G domains with all parallel-spin bonds across the DW, labeled as FM_X configuration, is also highlighted. (b),(c) Mn offcentering profile when the magnetic domain wall is assumed to be on top of the ferroelastic twin boundary [(b) DW+MW] and of the bulk lattice structure [(c) MW], compared to the single AFM-G magnetic domain with ferroelastic twin wall (dotted lines).

magnetic exchanges can then be inferred by mapping total energies—as obtained by enforcing the AFM-G optimal lattice structure—onto a Heisenberg model with normalized spins, $H = \sum_{ij} J_{ij} S_i S_j$. We assumed nearest-neighbor interactions J_x, J_y, J_z and isotropic next-nearest-neighbor interaction J_2 across each interface in the supercell, plus a nearest-neighbor exchange J_x' between two Mn ions belonging to first and second MnO_2 layers from the twin boundary. Our results (see Table I) show a trend which agrees with the one previously reported for *Pnma* perovskites $BiFeO_3$ and $LaFeO_3$ [32]. As the Mn-O-Mn angle θ is reduced when moving away from the DW, the exchange coupling component perpendicular to the twin wall decreases ($J_x' < J_x$). More generally,

TABLE I. Heisenberg exchange coupling constants (in meV) and corresponding structural information, i.e., Mn-O-Mn bond angle θ and Mn-O bond length d. Bulk values are also reported in parentheses, in qualitative good agreement with previous findings [31].

	J_x	J_y	J_z	J_x'	J_2
	11.13	18.34	18.42	7.61	1.63
	(7.44)	(7.44)	(10.79)	(7.44)	(1.80)
θ (deg)	158.2	160.5	158.7	157.7	
	(156.3)	(156.3)	(158.1)	(156.3)	
d (Å)	1.91	1.9–1.91	1.89–1.91	1.92	
	(1.92)	(1.92)	(1.91)	(1.92)	

the structural-induced strong modifications observed in the anisotropic exchange constants can be qualitatively understood assuming $J \propto t_{pd}^4 \cos^2\theta/[\Delta^2(2\Delta + U_{oxy})]$, where t_{pd} describes the overlap integral between Mn-d and O-p states, Δ is the $d^3 \rightarrow d^4\underline{L}$ charge transfer energy and U_{oxy} the on-site correlation energy on O ions [33,34]. Exchange couplings are strongly affected by both the Mn-O-Mn angle (increasing as $\theta \rightarrow 180^\circ$) and the Mn-O bond length d, where $t_{pd} \propto d^{-g}$ and $g = 3.5$ [35]. From this parametrization, an offcentering of Mn ions is also expected to enhance the corresponding exchange interaction; in fact, assuming that a distortion u induces a hybridization change $\Delta t_{pd} \sim \pm gu + g(g+1)u^2/2$, one immediately finds that $J \propto t_-^2 t_+^2 \sim t_{pd}^4(1 + gu^2)$.

On the other hand, different local spin configurations at the boundary strongly influence the structural deformations, hence the polarization profiles. Indeed, in the presence of both a magnetic wall (the so-called FM_X configuration) and a structural twin boundary, the offcentering of relaxed Mn ions is strongly reduced along the Y direction, while it is almost doubled along the X direction, in order to decrease the magnetic energy cost of having parallel spin bonds across the domain wall [see Fig. 4(b)]. Interestingly, this kind of spin-phonon coupling is expected to show up also in the presence of a MW in a structural (ferroelastic) monodomain; in fact, we predict an antiferroelectric-like profile of Mn offcenterings at the boundary enforcing the FM_X spin configuration on top of a bulk lattice structure, with no twin boundaries [see Fig. 4(c)]. Furthermore, the corresponding MW energy $E_{MW} \sim 7.2\ \mathrm{mJ/m^2}$ is slightly larger than the additional energy cost of having the magnetic wall pinned at the twin wall. We additionally note that, unfortunately, almost all the considered spin configurations do not display a net interface magnetization, due to perfect compensation of magnetic moments along different directions. On the other hand, a truly ferromagnetic (FM) interface, that in principle could be moved and controlled by applying an external magnetic field, is realized in the FM spin configuration, with all FM bonds around the boundary, with an estimated rise of the energy of $\sim$0.7 eV per layer. However, an alternative possibility to engineer a FM ferroelectric DW, that is left for future analysis, would be that of having a local canting of spins at the wall, giving rise to weak FM moments.

IV. CONCLUSIONS

In conclusion, we have performed an accurate analysis from first principles of (multi)ferroic domain walls in prototypical orthorhombic perovskites $CaTiO_3$ and $CaMnO_3$. We have shown that twin boundaries and domain walls, which naturally occur in ferroic materials, can indeed host features which do not appear in the corresponding bulk. Specifically, we propose that the predicted and observed twin-wall polarization in CTO has a hybrid improper origin arising from a cooperative interplay of rotational distortions acting on both the A-site and B-site cations. In this picture, the existence of a secondary FE instability is substantially reflected only in the anomalous Born effective charges of B-site ions, which cause a significant contribution to wall $\boldsymbol{P}$ even for small offcenterings. However, we argue that DW polar ionic displacements are primarily determined by two interfacing antipolar structures with different polarities, and as such they are strongly locked to the local pattern of AFD distortions. In confirmation of this scenario, we found that similar DW features, i.e., a significant offcenter of cations La and Fe along the supercell Y axis, develop in $LaFeO_3$, which displays in the bulk the same AFD distortions as CTO and CMO but no FE instability involving Fe-ions offcentering. Furthermore, a very recent TEM experiment unveiled the existence of polar distortions at antiphase boundaries of $PbZrO_3$, an antiferroelectric orthorhombic perovskite with similar rotation and tilting distortions, which have been explained in terms of a general Landau theory approach to ferroelectricity at antiferroelectric domain walls [36]. Finally, our results suggest that the coexistence of ferroelectricity and magnetism as arising by the very same ions is indeed possible, putting forward CMO as a possible material where multiferroic nanoscopic features can appear at its twin walls, and eventually suggesting a new route to engineer multiferroicity in single-phase materials. Even though the DW ferroic properties do not seem to be switchable, due to their improper origin, they can in principle provide additional handles to control and move domain walls beside conventional mechanical-based mechanisms.

ACKNOWLEDGMENTS

We thank Dr. J. Íñiguez for fruitful discussions and useful insights about cooperative oxygen rotations and antiferroelectric distortions. We acknowledge the MIUR-PRIN project "Interfacce di ossidi: nuove proprieta' emergenti, multifunzionalita' e dispositivi per l'elettronica e l'energia (OXIDE)", and PRACE for awarding us access to resource MareNostrum based in Spain at Barcelona Supercomputing Center (BSC-CNS).

[1] S. Wada, K. Yako, K. Yokoo, H. Kakemoto, and T. Tsurumi, Ferroelectrics **334**, 17 (2006).
[2] E. K. H. Salje, Chem. Phys. Chem. **11**, 940 (2010).
[3] E. K. H. Salje, Annu. Rev. Mater. Res. **42**, 265 (2012).
[4] G. Catalan, J. Seidel, R. Ramesh, and J. F. Scott, Rev. Mod. Phys. **84**, 119 (2012).
[5] W. T. Lee, E. K. H. Salje, and U. Bismayer, J. Appl. Phys. **93**, 9890 (2003).
[6] W. T. Lee, E. K. H. Salje, and U. Bismayer, J. Phys.: Condens. Matter **15**, 1353 (2003).
[7] E. K. H. Salje, *Phase Transition in Ferroelastic and Co-Elastic Crystals* (Cambridge University Press, Cambridge, UK, 1993).
[8] L. Goncalves-Ferreira, S. A. T. Redfern, E. Artacho, and E. K. H. Salje, Phys. Rev. Lett. **101**, 097602 (2008).
[9] E. Cockayne and B. P. Burton, Phys. Rev. B **62**, 3735 (2000).
[10] S. Bhattacharjee, E. Bousquet, and P. Ghosez, Phys. Rev. Lett. **102**, 117602 (2009).

[11] P. Barone, S. Kanungo, S. Picozzi, and T. Saha-Dasgupta, Phys. Rev. B **84**, 134101 (2011).
[12] J. M. Rondinelli, A. S. Eidelson, and N. A. Spaldin, Phys. Rev. B **79**, 205119 (2009).
[13] I. B. Bersuker, Phys. Rev. Lett. **108**, 137202 (2012).
[14] N. A. Hill, J. Phys. Chem. B **104**, 6694 (2000).
[15] H. Sakai, J. Fujioka, T. Fukuda, D. Okuyama, D. Hashizume, F. Kagawa, H. Nakao, Y. Murakami, T. Arima, A. Q. R. Baron *et al*., Phys. Rev. Lett. **107**, 137601 (2011).
[16] T. Günter, E. Bousquet, A. David, P. Boullay, P. Gho sez, W. Prellier, and M. Fiebig, Phys. Rev. B **85**, 214120 (2012).
[17] S. Van Aert, S. Turner, R. Delville, D. Schryvers, G. Van Tendeloo, and E. K. H. Salje, Adv. Mater. **24**, 523 (2012).
[18] N. A. Benedek and C. J. Fennie, Phys. Rev. Lett. **106**, 107204 (2011).
[19] J. M. Rondinelli and C. J. Fennie, Adv. Mater. **24**, 1961 (2012).
[20] L. Bellaiche and J. Íñiguez, Phys. Rev. B **88**, 014104 (2013).
[21] J. P. Perdew, A. Ruzsinszky, G. I. Csonka, O. A. Vydrov, G. E. Scuseria, L. A. Constantin, X. Zhou, and K. Burke, Phys. Rev. Lett. **100**, 136406 (2008).
[22] G. Kresse and D. Joubert, Phys. Rev. B **59**, 1758 (1999).
[23] S. F. Matar, Prog. Solid State Chem. **31**, 239 (2003).
[24] V. Gopalan and D. B. Litvin, Nature Mater. **10**, 376 (2011).
[25] A. M. Glazer, Acta Crystallogr. **B28**, 3384 (1972).
[26] The DW energies are computed as $E_{DW} = (E - E_0)/2S$, where E is the energy of the DW configuration, E_0 the energy of the bulk structure evaluated for the same supercell, and S is the surface area of the cell parallel to the DW. The factor 2 comes from the presence of two DWs in the supercell.
[27] In other words, rotations around the pseudocubic X axis appear to be in-phase just at the DW, whereas rotations around pseudocubic axes Y, Z remain out-of-phase and in-phase, respectively; the local pattern of rotations around the DW would correspond then to a $b^+a^-c^+$ Glazer's configuration.
[28] B. Meyer and D. Vanderbilt, Phys. Rev. B **65**, 104111 (2002).
[29] In order to further verify the B ions offcentering caused by the AFD distortions, we also performed a calculation where the A ions have been fixed to their centrosymmetric positions (without antipolar distortions) and oxygens to their optimal positions (i.e., in the ground-state rotational pattern). When B ions are allowed to relax from the centrosymmetric position, they adopt a distorted pattern qualitatively consistent with the fully optimized structure, even though their absolute offcentering is reduced to $\sim$1 pm at the CTO DW.
[30] J. Hong, A. Stroppa, J. Íñiguez, S. Picozzi, and D. Vanderbilt, Phys. Rev. B **85**, 054417 (2012).
[31] M. Nicastro and C. H. Patterson, Phys. Rev. B **65**, 205111 (2002).
[32] C. Weingart, N. Spaldin, and E. Bousquet, Phys. Rev. B **86**, 094413 (2012).
[33] A. J. Millis, Phys. Rev. B **55**, 6405 (1997).
[34] H. Meskine, H. König, and S. Satpathy, Phys. Rev. B **64**, 094433 (2001).
[35] W. A. Harrison, *Electronic Structure and the Properties of Solids* (Freeman, San Francisco, 1980).
[36] X.-K. Wei, A. K. Tagantsev, A. Kvasov, K. Roleder, C.-L. Jia and N. Setter, Nature Commun. **5**, 3031 (2014).